Acta Mech. Sin. (2011) 27(6):938–949
DOI 10.1007/s10409-011-0520-2

RESEARCH PAPER

Geometric and material nonlinear analysis of tensegrity structures

Hoang Chi Tran · Jaehong Lee

Received: 17 March 2011 / Revised: 9 July 2011 / Accepted: 13 July 2011

Abstract A numerical method is presented for the large deflection in elastic analysis of tensegrity structures including both geometric and material nonlinearities. The geometric nonlinearity is considered based on both total Lagrangian and updated Lagrangian formulations, while the material nonlinearity is treated through elastoplastic stress–strain relationship. The nonlinear equilibrium equations are solved using an incremental-iterative scheme in conjunction with the modified Newton–Raphson method. A computer program is developed to predict the mechanical responses of tensegrity systems under tensile, compressive and flexural loadings. Numerical results obtained are compared with those reported in the literature to demonstrate the accuracy and efficiency of the proposed program. The flexural behavior of the double layer quadruplex tensegrity grid is sufficiently good for lightweight large-span structural applications. On the other hand, its bending strength capacity is not sensitive to the self-stress level.

Keywords Nonlinear analysis · Tensegrity structures · Geometric nonlinearity · Material nonlinearity · Large displacements

1 Introduction

Over the past few decades, tensegrity structures first proposed by Fuller [1] have attracted considerable attention in a wide diversity of fields including aerospace [2], architecture [3,4], civil engineering [5–7], biology [8–11], mathematics [12,13] and robotics [14,15]. They belong to a class of free-standing pre-stressed pin-jointed cable-strut system where contacts are allowed among the struts [16]. Their classification is presented as Class 1 (where bars do not touch) and Class 2 (where bars do connect to each other at a pivot) [17,18]. A complete analysis of the tensegrity systems comprises two steps; the first one is form-finding which is the process of finding an equilibrium configuration; and the second is the study of behavior under external loads. Many researchers have made important contributions to the form-finding step in which Tibert and Pellegrino [19] classified the existing methods into two categories: kinematical methods and statical methods. Analysis step for behavior is still a difficult issue for structural engineers since tensegrity systems are in general both kinematically and statically indeterminate. Kebiche et al. [5] presented a geometrical nonlinear elastic analysis for a basic quadruplex module (four-strut tensegrity prism) subjected to axial, flexural and torsional loads and a five-quadruplex module tensegrity system under traction based on total Lagrangian formulation. Kahla and Kebiche [20] presented both geometrically nonlinearity and elastoplastic analysis of a five-quadruplex module tensegrity beam using an updated Lagrangian formulation. Recently, Murakami [21] investigated the elastic behavior of a three-strut tensegrity module under static load at various pre-stress levels by applying the updated Lagrangian formulation. More recently, using a set of well-chosen generalized coordinates and the virtual work approach Crane III et al. [22] developed a mathematical model derivation addressing the static analysis problem and found the displacements of the structure under applied external forces. The research was performed for only three- and four-strut tensegrities based on regular prisms. For more complex structures, numerical method has to be considered.

The objective of this paper is to investigate the behavior of tensegrity systems considering both geometric and material nonlinearities when they are subjected to various types of loadings by using both total Lagrangian and updated Lagrangian formulations. In order to capture the structural behavior, principle of virtual work by Bathe et al. [23], Bathe

H.C. Tran · J. Lee (✉)
Department of Architectural Engineering,
Free Form Architecture Institute, Sejong University,
98 Kunja Dong, Kwangjin Ku,
Seoul 143-747, Korea
e-mail: jhlee@sejong.ac.kr

and Ozdemir [24] and Bathe [25] including both geometric and material nonlinearities for a truss element is applied with an incremental-iterative solution strategy in conjunction with the modified Newton–Raphson method. Two types of analyses are put forward, i.e. geometric nonlinear elastic and geometric nonlinear elastoplastic analyses. Response of a quadruplex module in a state of self-stress under tension, compression and flexure is studied, as well as behavior characterization of a double layer quadruplex tensegrity grid and a five-quadruplex module tensegrity beam. The influence of the self-stress level is investigated. A comparison between the two formulations is also presented based on the results obtained. The updated Lagrangian formulation is recommended for the large deflection analysis of tensegrity structures.

2 Fundamental assumptions and constitutive modeling of element behavior

2.1 Fundamental assumptions

In establishing the stress–strain relation to account for yielding behavior of an axially-loaded bar, the following assumptions are adopted for tensegrity structures:

(1) Members are connected by pin joints;

(2) The cross-sectional area of each member remains unchanged during the deformation process;

(3) Buckling of the strut is not considered;

(4) There are no dissipative forces acting on the system.

2.2 Constitutive modeling of element behavior

The elastoplastic stress–strain relationship (Fig. 1) to model linear elastic and yielding behavior of a truss element can be expressed as

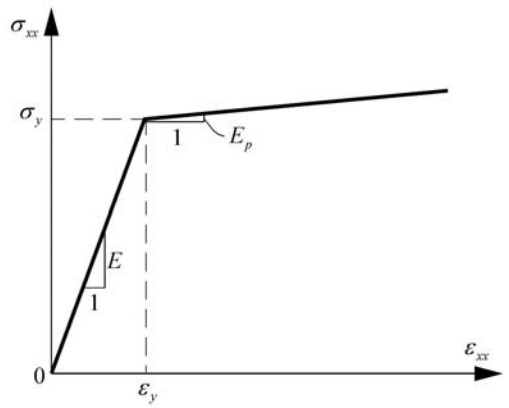

Fig. 1 Engineering stress–strain constitutive model for elastoplastic material

$$\sigma_{xx} = \begin{cases} E\varepsilon_{xx}, & \text{if } \sigma_{xx} < \sigma_y, \\ f(\varepsilon_{xx}), & \text{if } \sigma_{xx} \geq \sigma_y, \end{cases} \tag{1}$$

where ε_{xx}, σ_{xx}, σ_y and E are the engineering axial strain, stress, yield stress and the essential elastic modulus, respectively. $f(\varepsilon_{xx})$ is a one-dimensional plastic flow rule. Regarding cable element, $f(\varepsilon_{xx})$ is defined by experiment whereas for strut, it is assumed to exhibit elastic-ideal plastic behavior (i.e., $f(\varepsilon_{xx}) = \sigma_y$).

3 Finite element model

In an incremental-iterative analysis, three typical configurations can be identified for the structure under consideration: the self-stressed initial undeformed configuration C_0, the last calculated deformed configuration C_1 and the current deformed configuration C_2 (Fig. 2). In this paper, the left superscript of a symbol is used to indicate the configuration in which the quantity occurs, and the left subscript indicates the configuration to which the quantity is referred. Those quantities generated as increments within the step from C_1 to C_2 will be denoted with no left superscript. And an index j has the values of zero and unity ($j = 0, 1$) unless otherwise mentioned. The quantities in the equation established by the total Lagrangian (TL) formulation and the updated Lagrangian (UL) formulation will be referred to C_0, C_1, respectively.

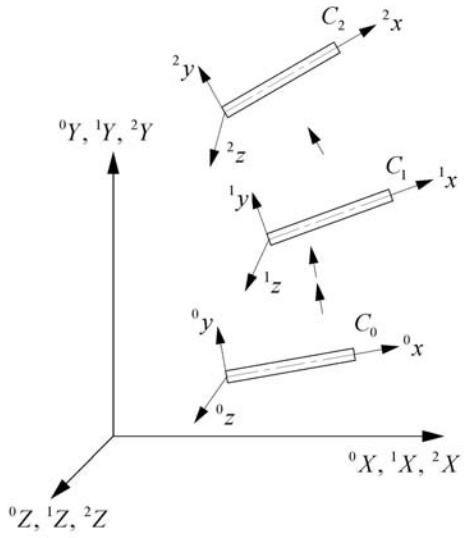

Fig. 2 Reference and deformed configurations of a body in three dimensions

By the TL formulation, the virtual work equation of equilibrium by Bathe [25] for a space truss element at C_2 can be linearized and referred to C_0, as

$$\int_{{}_0V} {}_0E_0e_{xx}\delta({}_0e_{xx})\mathrm{d}^0V + \int_{{}_0V} {}^1_0S_{xx}\delta({}_0\eta_{xx})\mathrm{d}^0V = {}^2_0R - \int_{{}_0V} {}^1_0S_{xx}\delta({}_0e_{xx})\mathrm{d}^0V. \quad (2)$$

Similarly, by the UL formulation, the virtual work equation of equilibrium by Bathe [25] for a space truss element at C_2 can be linearized and referred to C_1, as

$$\int_{{}_1V} {}_1E_1e_{xx}\delta({}_1e_{xx})\mathrm{d}^1V + \int_{{}_1V} {}^1\tau_{xx}\delta({}_1\eta_{xx})\mathrm{d}^1V = {}^2_1R - \int_{{}_1V} {}^1\tau_{xx}\delta({}_1e_{xx})\mathrm{d}^1V, \quad (3)$$

where ${}_je_{xx}\left(= \dfrac{\partial u}{\partial {}^jx}\right)$ is a linear strain; ${}_j\eta_{xx}\left(= \dfrac{1}{2}\left(\dfrac{\partial u}{\partial {}^jx}\right)^2 + \dfrac{1}{2}\left(\dfrac{\partial v}{\partial {}^jx}\right)^2 + \dfrac{1}{2}\left(\dfrac{\partial w}{\partial {}^jx}\right)^2\right)$ is a nonlinear strain; u, v and w are centroidal displacements of the element in its local coordinate in x-, y- and z-directions, respectively; ${}_1E\left(= {}_0E\left(\dfrac{{}^1L}{{}_0^1L}\right)^3\right)$ is a tangent modulus; ${}^jL$ and ${}^jV$ are the length and the volume of an element, respectively; ${}^1_0S_{xx}$ and ${}^1\tau_{xx}$ are 2nd Piola–Kirchhoff and Cauchy stress, respectively; the Cauchy stress can be related to the 2nd Piola–Kirchhoff stress by ${}^1\tau_{xx} = {}^1_0S_{xx}\left(\dfrac{{}^1L}{{}_0^1L}\right)$; and ${}^2_jR$ is the external virtual work.

The incremental strains of Eqs. (2) and (3) are, respectively, related to the Green–Lagrange strain ${}_0\varepsilon_{xx}$ and Almansi strain ${}_1\varepsilon_{xx}$ as

$${}_0\varepsilon_{xx} = \frac{\partial u}{\partial {}^0x} + \frac{1}{2}\left[\left(\frac{\partial u}{\partial {}^0x}\right)^2 + \left(\frac{\partial v}{\partial {}^0x}\right)^2 + \left(\frac{\partial w}{\partial {}^0x}\right)^2\right] = {}_0e_{xx} + {}_0\eta_{xx}, \quad (4a)$$

$${}_1\varepsilon_{xx} = \frac{\partial u}{\partial {}^1x} - \frac{1}{2}\left[\left(\frac{\partial u}{\partial {}^1x}\right)^2 + \left(\frac{\partial v}{\partial {}^1x}\right)^2 + \left(\frac{\partial w}{\partial {}^1x}\right)^2\right] = {}_1e_{xx} - {}_1\eta_{xx}. \quad (4b)$$

Substituting linear shape functions for the displacement variables, Eqs. (2) and (3) can be, respectively, derived for a single space truss element as

$$({}^1_0\boldsymbol{k}_e + {}^1_0\boldsymbol{k}_g)\Delta_0\boldsymbol{u} = {}^2_0\boldsymbol{f} - {}^1_0\boldsymbol{f}, \ \text{for TL}, \quad (5a)$$

$$({}^1_1\boldsymbol{k}_e + {}^1_1\boldsymbol{k}_g)\Delta_1\boldsymbol{u} = {}^2_1\boldsymbol{f} - {}^1_1\boldsymbol{f}, \ \text{for UL}, \quad (5b)$$

where ${}^1_j\boldsymbol{k}_e$ and ${}^1_j\boldsymbol{k}_g$ are element elastic and geometric stiffness matrices, respectively; $\Delta_j\boldsymbol{u}$ is element displacement increment vector, which consists of three translations at each node; ${}^2_j\boldsymbol{f}$ and ${}^1_j\boldsymbol{f}$ are external and internal element forces acting at C_2 and C_1, respectively. By the element assembly procedure, Eq. (5) can be constructed for the structure as

$$({}^1_0\boldsymbol{K}_E + {}^1_0\boldsymbol{K}_G)\Delta_0\boldsymbol{U} = {}^2_0\boldsymbol{P} - {}^1_0\boldsymbol{F}, \ \text{for TL}, \quad (6a)$$

$$({}^1_1\boldsymbol{K}_E + {}^1_1\boldsymbol{K}_G)\Delta_1\boldsymbol{U} = {}^2_1\boldsymbol{P} - {}^1_1\boldsymbol{F}, \ \text{for UL}. \quad (6b)$$

The final forms of the tangent stiffness matrices derived above are equivalent to those by Murakami [26], Masic et al. [27], Deng and Kwan [28], Zhang and Ohsaki [29] and Ohsaki and Zhang [30]. It should be noted that if an infinitesimal mechanism is applied to a tensegrity system, the material elastic stiffness $\boldsymbol{K}_E$ in Eq. (6) vanishes. Accordingly, its initial stiffness at the initial state (or the stability of the structure) involves with the geometric stiffness $\boldsymbol{K}_G$ only, which can be created by its self-stress modes.

4 Nonlinear solution method

The solution of nonlinear equations usually requires the use of an incremental-iterative solution scheme. In this paper, modified Newton–Raphson method is employed and expressed as

$${}^{(m)}{}^1_0\boldsymbol{K}_T\Delta_0\boldsymbol{U}^{(i)} = {}^{(m+1)}\lambda^{(i)}\boldsymbol{P} - {}^{(m+1)}{}^1_0\boldsymbol{F}^{(i-1)}, \ \text{for TL}, \quad (7a)$$

$${}^{(m)}{}^1_1\boldsymbol{K}_T\Delta_1\boldsymbol{U}^{(i)} = {}^{(m+1)}\lambda^{(i)}\boldsymbol{P} - {}^{(m+1)}{}^1_1\boldsymbol{F}^{(i-1)}, \ \text{for UL}, \quad (7b)$$

where ${}^{(m)}{}^1_j\boldsymbol{K}_T$ $\left(= {}^{(m)}{}^1_j\boldsymbol{K}_E + {}^{(m)}{}^1_j\boldsymbol{K}_G\right)$ is the tangent stiffness evaluated at C_1 for load level m referred to C_j; "m" is the beginning load level for the current, "$m+1$", load step; ${}_j\boldsymbol{U}$, $\boldsymbol{P}$ and ${}^1_j\boldsymbol{F}$ are the structure displacement, the reference external load and the equilibrated internal force vectors, respectively; λ is a load parameter; Δ symbolizes iterative change; and the parenthetical superscript signifies the iteration number. The accumulated incremental displacement vector and the load parameter through iteration "i" within incremental load step "$m+1$" are defined as

$$\mathrm{d}_j\boldsymbol{U}^{(i)} = \mathrm{d}_j\boldsymbol{U}^{(i-1)} + \Delta_j\boldsymbol{U}^{(i)}, \quad (8a)$$

$$\mathrm{d}\lambda^{(i)} = \mathrm{d}\lambda^{(i-1)} + \Delta\lambda^{(i)}, \quad (8b)$$

where $\mathrm{d}_j\boldsymbol{U}^{(0)} = \boldsymbol{0}$; $\mathrm{d}\lambda^{(0)} = 0$; and "d" symbolizes incremental change within the load step. Accumulated variable quantities through iteration "i" for incremental load step "$m+1$" are defined as

$${}^{(m+1)}{}_j\boldsymbol{U}^{(i)} = {}^{(m+1)}{}_j\boldsymbol{U}^{(i-1)} + \Delta_j\boldsymbol{U}^{(i)}, \quad (9a)$$

$${}^{(m+1)}\lambda^{(i)} = {}^{(m+1)}\lambda^{(i-1)} + \Delta\lambda^{(i)}, \quad (9b)$$

$${}^{(m+1)}{}^1_j\boldsymbol{F}^{(i)} = {}^{(m+1)}{}^1_j\boldsymbol{F}^{(i-1)} + \Delta^1_j\boldsymbol{F}^{(i)}, \quad (9c)$$

$${}^{(m+1)}{}_j\boldsymbol{R}^{(i)} = {}^{(m+1)}\lambda^{(i)}\boldsymbol{P} - {}^{(m+1)}{}^1_j\boldsymbol{F}^{(i)}, \quad (9d)$$

where ${}_j\boldsymbol{R}$ is the out-of-balance force vector. For "$i-1$" $= 0$, the variables are equal to those of the previous incremental step. For the solution of Eq. (7b) by UL formulation, it is required to update the nodal coordinate vector $\boldsymbol{X}$ to calculate the updated coordinate transformation matrices as

$${}^{(m+1)}\boldsymbol{X}^{(i)} = {}^{(m+1)}\boldsymbol{X}^{(i-1)} + \Delta_1\boldsymbol{U}^{(i)}. \quad (10)$$

The iterative process is repeated until the convergence condition is satisfied. The slackening of cable elements is treated in the following manner: the actual length of each cable is

computed and compared to its free length within each iteration. If the actual length is shorter than the free length, then the cable is slack. Its axial force is equal to zero and there is no contribution of its stiffness to the global structure one.

5 Numerical examples

5.1 Geometric nonlinear elastic analysis

5.1.1 A quadruplex module

A quadruplex system (Fig. 3) comprising four struts and 12 cables, which was studied by Kebiche et al. [5], is herein used for verification purpose. Three types of loading are considered: tension, compression and flexure (upward and downward). The influence of the self-stress level is also investigated. Before applying external load, the initial self-stress design procedure proposed by Tran and Lee [7] was performed to define the force density coefficient (force-to-length ratio) vector for the given and free-standing quadruplex system was performed. Note that the statically indeterminate foundation constraints (boundary conditions) are imposed in the manner which does not cause any effect on the self-equilibrium state of the system. Based on the rank deficiency of equilibrium matrix, the number of self-stress modes and infinitesimal mechanisms of this system are found to be one and three, respectively, as presented in Pellegrino and Calladine [31] and Tran and Lee [32].

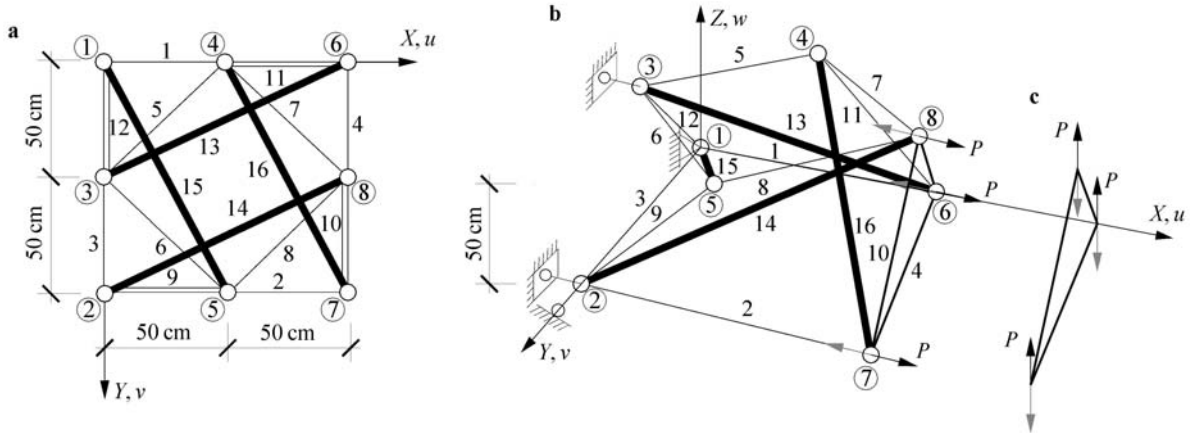

Fig. 3 The quadruplex module under tensile, compressive and flexural loads. **a** Plan view; **b** Tension compression; **c** Upward flexure downward flexure

It is observed from Eq. (6) that this single self-stress mode stiffens the infinitesimal mechanisms. In other words, the geometric stiffness $\boldsymbol{K}_G$ of the system induced by single self-stress mode exhibits positive stiffness to all directions within the infinitesimal displacements. Force density coefficients, initial self-stress values, geometrical and material properties of the quadruplex module are given in Table 1. The self-stress level (γ) in this case is equal to 55 N/cm. Concentrated loads are applied on Nodes 6, 7 and 8. The absolute value of displacement at the gravity center of the loaded cross-section (triangle 6,7,8) is plotted against the total applied loads for all loading cases.

(a) Tensile and compressive loads

As indicated in Fig. 3b, the tensile or compressive loads are applied on Nodes 6, 7 and 8 along the x-direction. The value of each load (P) varies from 0 to 2 kN. The present results, as plotted in Fig. 4, agree well with those of Ref. [5] for geometric nonlinear elastic analysis by using either TL or UL formulation. Furthermore, solutions obtained by the TL and UL formulations coincide with each other. The system becomes stiffer for increasing tension while it becomes softer for increasing compression.

(b) Flexural loads

Flexural loads (Fig. 3c) from 0 to 3.9 kN ($3P$) are applied on Nodes 6, 7 and 8 along the z-direction. The solutions (Fig. 5) by both formulations agree well with the results from Ref. [5]. Regardless of the load direction, the structure is stiffened as the external loads increase. The deformation in downward flexure is larger than that in upward flexure. This leads to the conclusion that the rigidity of lower "fibers" in the quadruplex system is larger than that of upper "fibers". From Figs. 4 and 5, it is clearly seen that the load-carrying capacity under tension and compression is better than that under flexure in the quadruplex system.

Table 1 Initial self-stress values, geometrical and material properties of the quadruplex module

Ele.	Nodes		Category	Force density coefficient/(daN·cm^{-1})	Length/cm	Initial self-stress/kN	Cross section/cm^2	Modulus/GPa
1	1	6	Lower	γ	5.5	100	5.5	0.280	40
2	2	7	cables	γ	5.5	100	5.5		
3	1	2		γ	5.5	100	5.5		
4	6	7		γ	5.5	100	5.5		
5	3	4	Upper	2γ	11.0	70.71	7.778 2	0.280	40
6	3	5	cables	2γ	11.0	70.71	7.778 2		
7	4	8		2γ	11.0	70.71	7.778 2		
8	5	8		2γ	11.0	70.71	7.778 2		
9	2	5	Bracing	2γ	11.0	70.71	7.778 2	0.280	40
10	7	8	cables	2γ	11.0	70.71	7.778 2		
11	4	6		2γ	11.0	70.71	7.778 2		
12	1	3		2γ	11.0	70.71	7.778 2		
13	3	6	Struts	-2γ	−11.0	122.47	−1.347 22	0.325	200
14	2	8		-2γ	−11.0	122.47	−1.347 22		
15	1	5		-2γ	−11.0	122.47	−1.347 22		
16	4	7		-2γ	−11.0	122.47	−1.347 22		

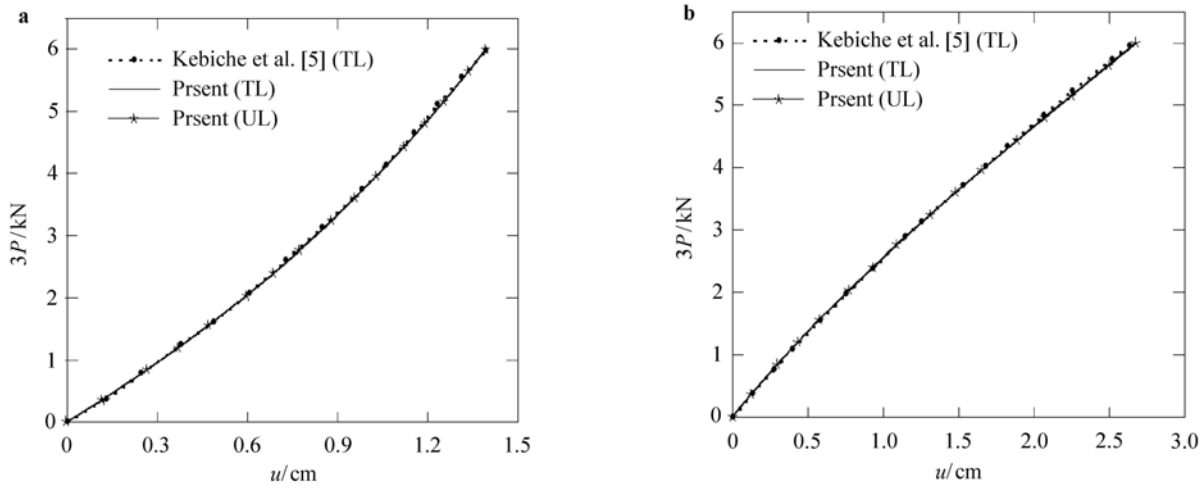

Fig. 4 Behavior of the quadruplex module under: **a** Tensile loads; **b** Compressive loads

(c) Influence of the self-stress level

Obviously, the stiffness of tensegrity system in Eq. (6) depends partly on the self-stress level. The influence of this level (γ = 2–9) on the behavior of the quadruplex system under tensile, compressive and flexural loads is investigated. Based on the load level, this γ's value range is so chosen as to avoid buckling in the strut. The relationship between the displacements in x- and z-directions (u, w) and the self-stress level (γ) are displayed in Figs. 6 and 7 for tensile, compressive and flexural loads, respectively. Total external load ($3P$) is assumed to be at a specified value, 4.5 kN.

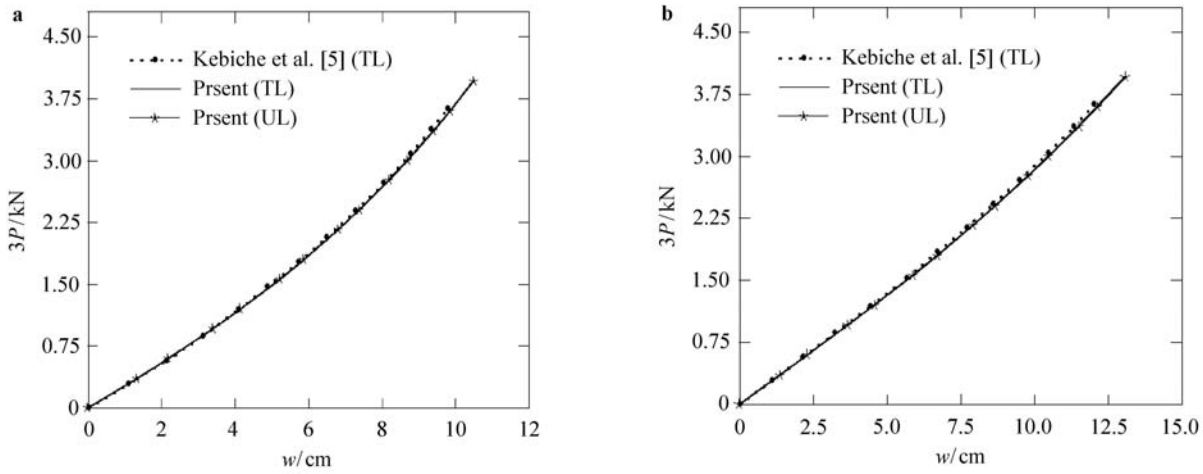

Fig. 5 Behavior of the quadruplex module under: **a** "Upward" flexural loads; **b** "Downward" flexural loads

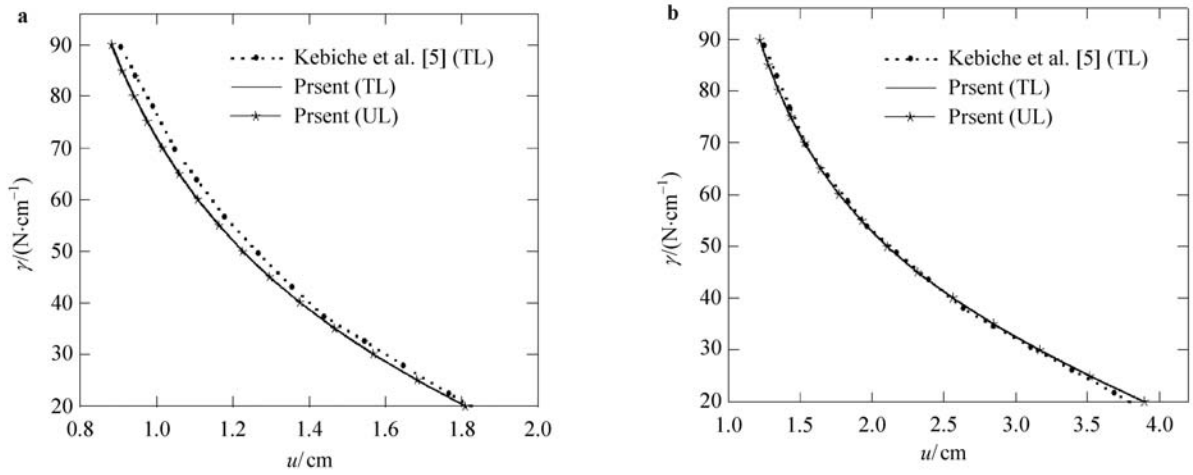

Fig. 6 Influence of the self-stress level on the quadruplex module under: **a** Tensile loads; **b** Compressive loads

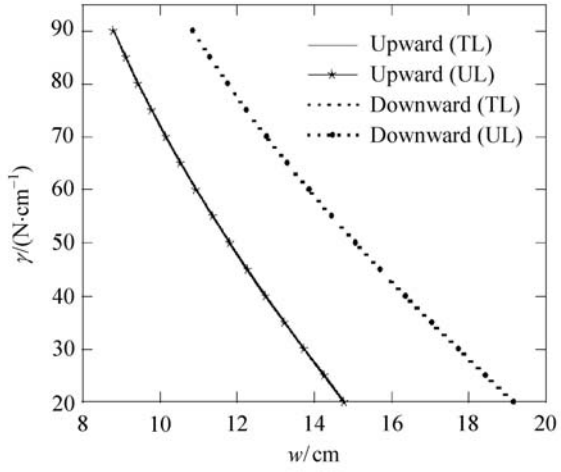

Fig. 7 Influence of the self-stress level on the quadruplex module under flexural loads

Figure 6 shows the comparison of the present results with those in Ref. [5]. In all cases, the displacement decreases when the self-stress level increases indicating that increasing the self-stress level makes the tensegrity system stiffer. This phenomenon becomes more sensitive for compressive loading. Figure 7 confirms that the lower "fibers" in the quadruplex system is more rigid than the upper "fibers". Figures 6 and 7 also confirm that load-carrying capacity under tension and compression is higher than that under flexure in the quadruplex system. The stiffness of both top and bottom surfaces of the module contributes to the module's global stiffness in the case of tensile and compressive loadings. While in the case of flexural loading they have little contribution to the module's global stiffness. It is observed from Figs. 6 and 7 that the results of two different formulations are in excellent agreement.

5.1.2 Double layer quadruplex tensegrity grid

Consider a tensegrity grid assembled from 20 (5×4) quadruplex modules (Fig. 3a) which consists of 79 nodes, 80 struts and 209 cables as described in Fig. 8. Similarly, in order to define the force density coefficient (force-to-length ratio) vector the initial self-stress design procedure proposed by Tran and Lee [7] was performed for the given and free-standing double layer quadruplex tensegrity grid before applying external load. Note that the statically indeterminate foundation constraints (boundary conditions) are imposed in the manner which causes no effect on the self-equilibrium states of the system. There exist 59 independent self-stress modes from the analysis of the equilibrium matrix of the system. The structure has only one infinitesimal mechanism when its six rigid-body motions are constrained, indicating that it is statically and kinematically indeterminate.

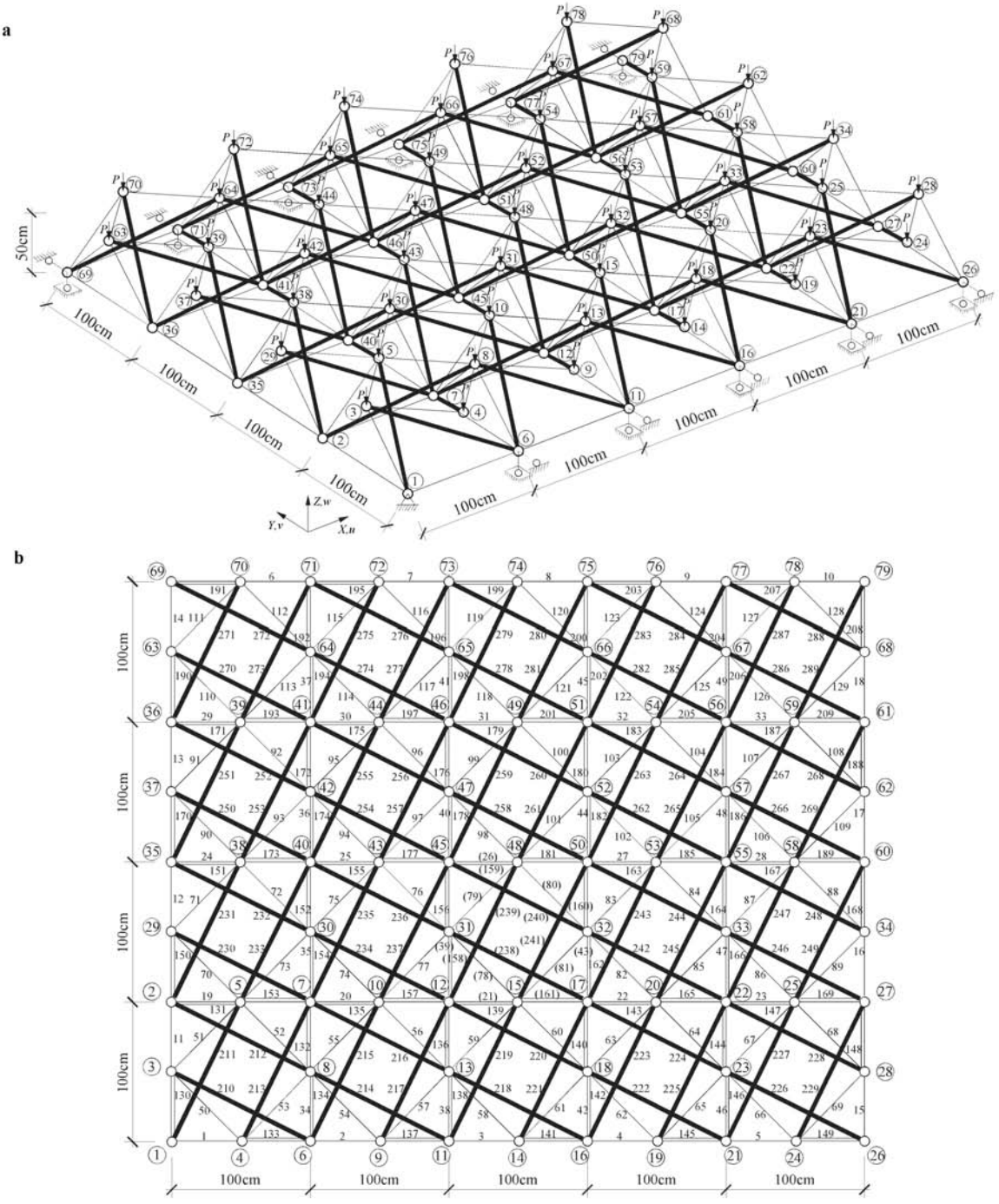

Fig. 8 A 20 (5 × 4) quadruplex module double layer tensegrity grid. **a** Perspective view; **b** Top view

According to the symmetry of the grid, all elements can be properly divided into seven groups as shown in Table 2 for the purpose of obtaining single integral feasible self-stress mode (see Tran and Lee [7] for more details). By imposing the constraint in which elements in the same group have the same force density coefficient (i.e., symmetric properties), the force density coefficients of seven groups and their corresponding initial self-stress values can be obtained and listed in Table 2. All the upper nodes of the double layer tensegrity grid are loaded by the same vertical downward load P.

Table 2 Initial single integral self-stress values of the 20 module quadruplex double layer tensegrity grid

Group No.	Ele.	Force density coefficient/(N·cm^{-1})		Initial self-stress/kN
1	1–10	γ	80	8.00
2	11–18	γ	80	8.00
3	19–33	2γ	160	16.00
4	34–49	2γ	160	16.00
5	50–129	2γ	160	113.137
6	130–209	2γ	160	113.137
7	210–289	-2γ	−160	−195.959

(a) Vertical loads

The vertical displacement w of node 48 against the applied load P for both TL and UL formulations is shown in Fig. 9. The global load-displacement behavior of the structure is nearly linear. The structure is softened as the external loads increase. The results of two formulations are in very good agreement. When the vertical load P reaches a value of 300 N, the maximum deflection (the vertical displacement of node 48) is 1.492 9 cm which is less than 1/250 of the short span. It indicates that the double layer quadruplex tensegrity grid is sufficiently good for lightweight large-span structural applications. However, a detailed study needs to be further conducted, which is beyond the scope of this paper. The axial force in typical elements is shown in Fig. 10. An average of 62% fall in tension (Fig. 10a) appears in the upper cables of 78 and 80 while a 19% average rise occurs in the lower cables of 39 and 43. An average of 10% increase in compression (Fig. 10b) occurs in all of typical struts (238–241).

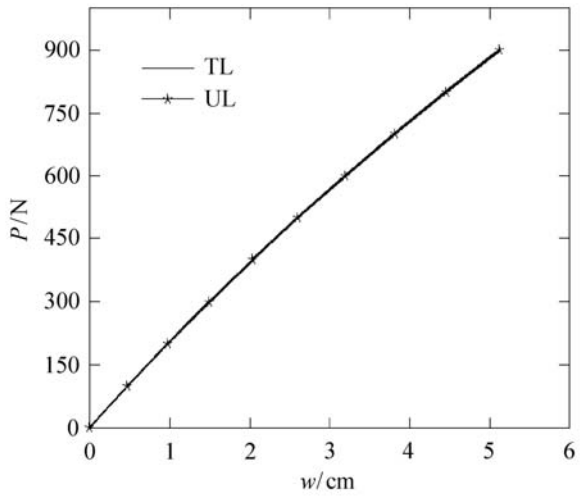

Fig. 9 The vertical displacement of node 48 against vertical loads in the double layer quadruplex tensegrity grid

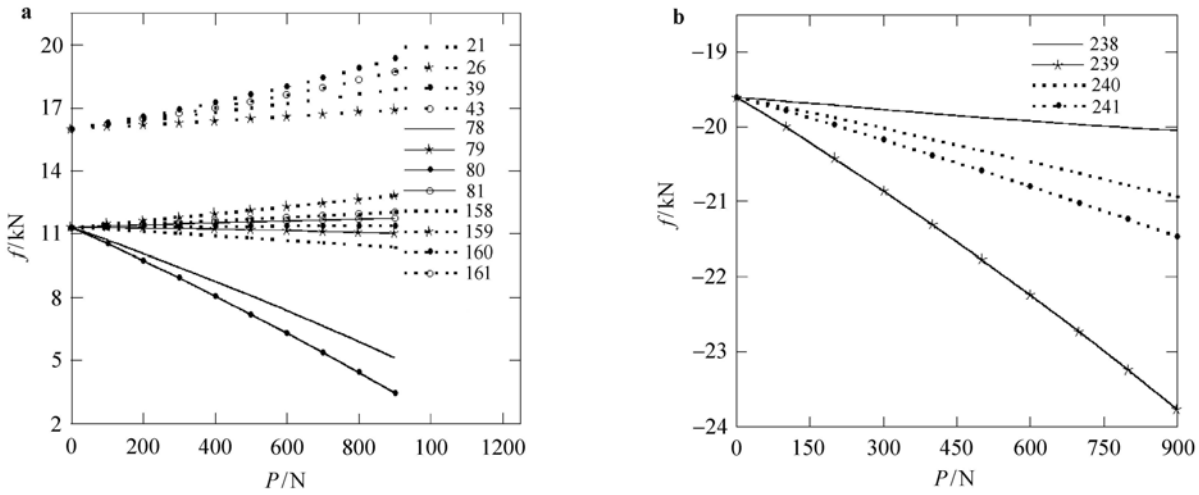

Fig. 10 Typical element axial forces. **a** Tensile forces in cables; **b** Compressive forces in struts

(b) Influence of the self-stress level

The influence of the self-stress level (γ = 2–9) on the behavior of the double layer quadruplex tensegrity grid is investigated for a specified value of the uniform vertical load P(= 300 N) on every node is investigated. The relationship between the vertical displacement (w) at node 48 and the self-stress level (γ) is displayed in Fig. 11. When γ increases from 2 to 9, the vertical deflection of the structure decreases by 6% only. Accordingly, the bending strength capacity of the double layer quadruplex tensegrity grid is not sensitive to the self-stress level. In other words, the increment of self-stress level contributes little to the bending stiffness of the structure.

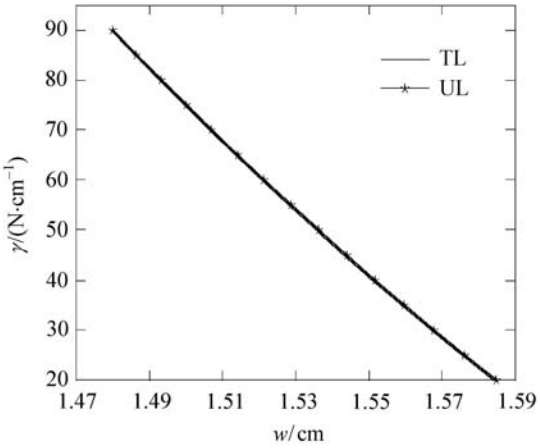

Fig. 11 Influence of the self-stress level on the behavior of the double layer quadruplex tensegrity grid under vertical loads

5.2 Geometric nonlinear elastoplastic analysis

The five-module (numbered from M1 to M5) tensegrity beam (Fig. 12) analyzed by Kahla and Kebiche [20] is considered. The quadruplex system shown in Fig. 3 is chosen as a unit module. Eight infinitesimal mechanisms and nine independent self-stress modes are determined based on the rank deficiency of equilibrium matrix for the tensegriy beam. Eight modes are from the beam itself. The last one, in which only Element 2 of each module is pre-stressed, is caused by the nonzero reaction forces due to the statically indeterminate supports at Nodes 2 and 27 in the x-direction. The aim of this mode is to strengthen the bending stiffness of the tensegrity beam.

In order to eliminate all the infinitesimal mechanisms, this tensegrity beam should be in the integral feasible self-stress mode which is a linear combination of the above nine independent self-stress modes (Tran and Lee [7]). The initial integral self-stress values and material properties for all elements of the beam are presented in Table 3. The experimental stress–strain relationship of cable elements (Fig. 13) proposed in Ref. [20] is adopted in this study, which shows yield stress σ_y = 480 MPa and rupture stress σ_r = 750 MPa corresponding to yield strain ε_y = 1.2% and rupture strain ε_r = 3.3%, respectively. Here struts are assumed to exhibit an elastic-ideal plastic behavior. All the upper nodes of this tensegriy beam are loaded by the same vertical downward load P, and the self-weight of the beam is also taken into account. The unit weight of the cable and the strut are 0.020 5 N/cm and 0.279 N/cm, respectively.

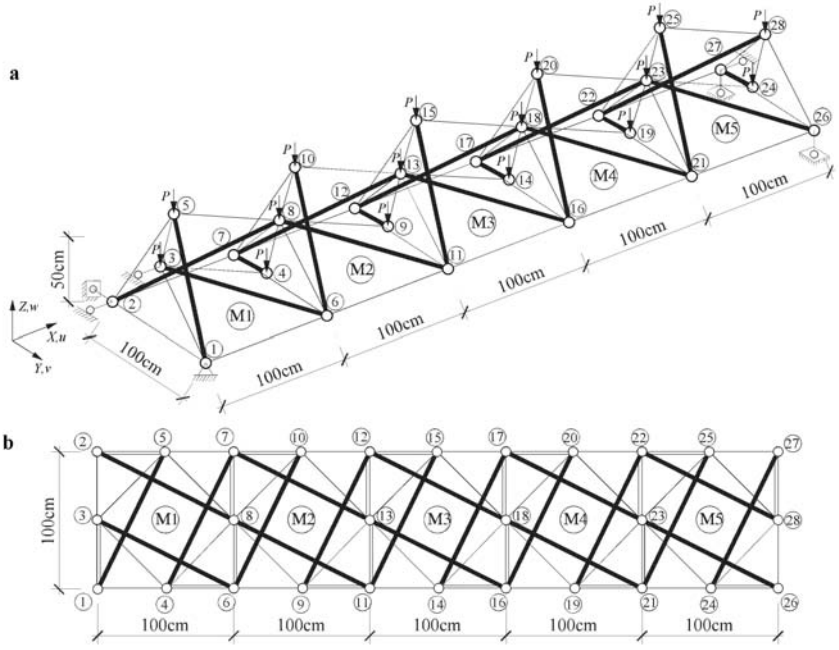

Fig. 12 A 5 quadruplex module tensegrity beam under vertical loads. **a** Perspective view; **b** Top view

Table 3 Initial integral self-stress values and material properties of the 5 module quadruplex tensegrity beam

Ele.	Category	Module 1/ kN	Module 2/ kN	Module 3/ kN	Module 4/ kN	Module 5/ kN	Cross section/ cm^2	Modulus/ GPa	Yield stress/ GPa
1	Lower	3.889	3.753	3.723	3.679	3.719	0.280	40	0.480
2	cables	6.870	6.517	6.552	6.559	6.963			
3		3.700	7.253	6.875	6.913	6.913			
4		7.253	6.875	6.913	6.913	3.705			
5	Upper	5.173	4.639	4.681	4.639	5.180	0.280	40	0.480
6	cables	5.158	5.040	5.053	5.040	5.180			
7		5.129	4.639	4.681	4.639	5.180			
8		5.250	5.084	5.095	5.084	5.180			
9	Bracing	5.262	5.084	5.095	5.084	5.180	0.280	40	0.480
10	cables	4.950	4.459	4.488	4.671	5.180			
11		5.158	4.639	4.681	4.639	5.180			
12		5.233	5.158	5.312	5.296	5.477			
13	Struts	−9.063	−8.472	−8.514	−8.472	−9.041	3.250	200	0.235
14		−9.063	−8.472	−8.514	−8.472	−8.971			
15		−9.063	−8.780	−8.776	−8.780	−8.971			
16		−8.934	−8.034	−8.108	−8.034	−8.971			

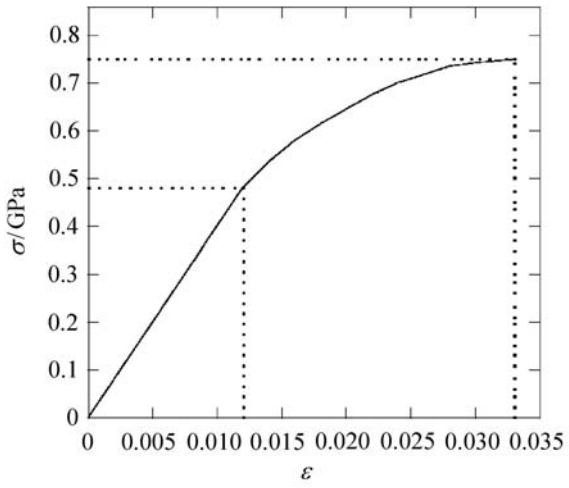

Fig. 13 Experimental stress–strain constitutive model of cable element [20]

Figure 14 shows the vertical displacement w of node 14 against applied load P computed using the two types of analyses, i.e. geometric nonlinear elastic and geometric nonlinear elastoplastic ones for both TL and UL formulations. As can be seen in Fig. 14, a good agreement is found between the present results and those of Ref. [20]. The predicted critical load by the UL formulation is P_{cr} = 1 181 N compared to 1 175 N given by Ref. [20]. Using the TL formulation, the structure is still sustainable at this load level. Another observation from Fig. 14 is that rather small difference can be seen between the results based on the two formulations. The vertical displacements obtained by geometric nonlinear elastic analysis are smaller than those obtained by geometric nonlinear elastoplastic analysis in both formulations at the same external load level.

6 Concluding remarks

A numerical method implemented into a computer program has been proposed for the large deflection inelastic analysis of tensegrity systems by using both the total Lagrangian and updated Lagrangian descriptions. Both geometric and material nonlinearities have been taken into account. Two types of analyses, i.e. geometric nonlinear elastic and geometric nonlinear elastoplastic ones are put forward. The proposed program traces the responses of the quadruplex unit module, the double layer quadruplex tensegrity grid and the five-quadruplex module tensegrity beam under external loads. From the numerical results obtained, the following conclusions can be made:

(1) The response of tensegrity structures has been observed to show a geometric stiffening, and the stiffness of tensegrity structures increases with the self-stress level.
(2) Regarding the quadruplex unit module, the stretching stiffness is dominated rather than the bending one.

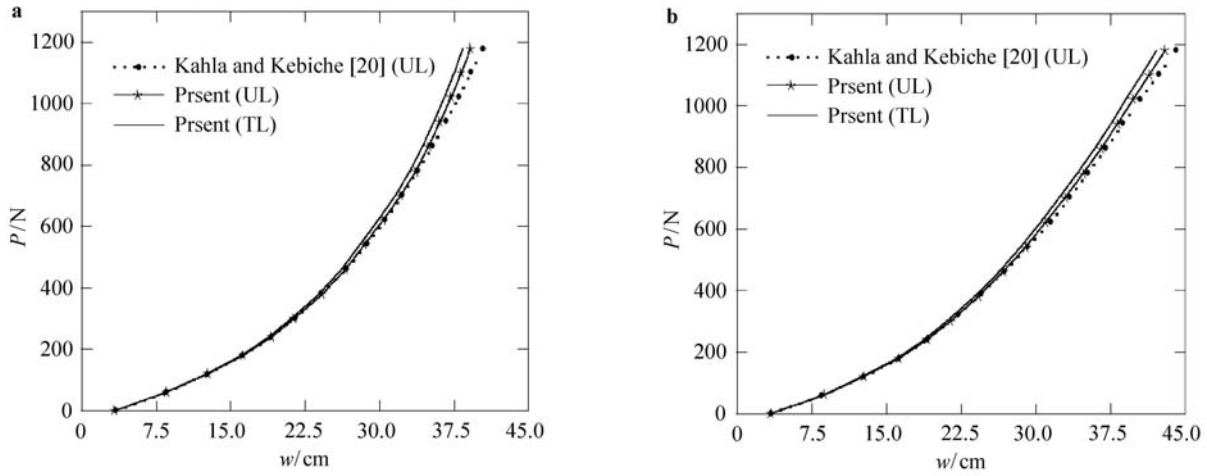

Fig. 14 The vertical displacement of node 14 against vertical loads in the 5 quadruplex module tensegrity beam by: **a** Geometric nonlinear elastic analysis; **b** Geometric nonlinear elastoplastic analysis

(3) The flexural behavior of the double layer quadruplex tensegrity grid is sufficiently good for lightweight large-span structural applications. On the other hand, its bending strength capacity is not sensitive to the self-stress level.
(4) It can be concluded that the proposed program can accurately predict the geometric and material nonlinear behavior of the tensegrity grid structures by using both total and updated Lagrangian descriptions.

Additional research including buckling of struts and dynamic behavior of tensegrity systems awaits further attention.

Acknowledgments The support of the research reported here by Basic Science Research Program through the National Research Foundation of Korea (NRF) funded by the Ministry of Education, Science and Technology (NRF2010-0019373) is gratefully acknowledged. The authors also would like to thank the anonymous reviewers for their suggestions in improving the standard of the manuscript.

References

1 Fuller, R.B.: Synergetics-Explorations in the Geometry of Thinking. Macmillan Publishing Co. Inc., London, UK (1975)
2 Tibert, A.G., Pellegrino, S.: Deployable tensegrity reflectors for small satellites. J. Spacecraft Rockets **39**(5), 701–709 (2002)
3 Fu, F.: Structural behavior and design methods of tensegrity domes. J. Constr. Steel Res. **61**(1), 23-35 (2005)
4 Tran, H.C., Lee, J.: Initial self-stress design of tensegrity grid structures. Comput. Struct. **88**(9-10), 558–566 (2010)
5 Kebiche, K., Kazi-Aoual, M.N., Motro, R.: Geometrical nonlinear analysis of tensegrity systems. Eng. Struct. **21**(9), 864–876 (1999)
6 Rhode-Barbarigos, L., Ali, N.B.H., Motro, R., et al.: Designing tensegrity modules for pedestrian bridges. Eng. Struct. **32**(4), 1158–1167 (2010)
7 Tran, H.C., Lee, J.: Self-stress design of tensegrity grid structures with exostresses. Int. J. Solids Struct. **47**(20), 2660–2671 (2010)
8 Ingber, D.E.: The architecture of life. Sci. Am. **278**(1), 48–57 (1998)
9 Ingber, D.E.: Tensegrity I. Cell structure and hierarchical systems biology. J. Cell Sci. **116**(7), 1157–1173 (2003)
10 Stamenovic, D.: Effects of cytoskeletal prestress on cell rheological behavior. Acta Biomater. **1**(3), 255–262 (2005)
11 Feng, X.Q., Li, Y., Cao, Y.P., et al.: Design methods of rhombic tensegrity structures. Acta Mech. Sinica **26**(4), 559–565 (2010)
12 Connelly, R., Whiteley, W.: Second-order rigidity and prestress stability for tensegrity frameworks. SIAM J. Discrete Math. **9**(3), 453–491 (1996)
13 Jórdan, T., Recski, A., Szabadka, Z.: Rigid tensegrity labelings of graphs. Eur. J. Combin. **30**(8), 1887–1895 (2009)
14 Paul, C., Lipson, H., Valero-Cuevas, F.: Design and control of tensegrity robots for locomotion. IEEE T. Robot. **22**(5), 944–957 (2006)
15 Rovira, A.G., Tur, J.M.M.: Control and simulation of a tensegrity-based mobile robot. Robot. Auton. Syst. **57**(5), 526–535 (2009)
16 Wang, B.B.: Free-standing Tension Structures: From Tensegrity Systems to Cable Strut Systems. Spon Press, London and New York (2004)
17 Pinaud, J.P., Solari, S., Skelton, R.E.: Deployment of a class 2 tensegrity boom. In: Proceedings of SPIE Smart Structures and Materials, SPIE Press 155–162 (2004)
18 Motro, R.: Tensegrity: Structural Systems for the Future. (1st edn.) Kogan Page Science, London (2003)
19 Tibert, A.G., Pellegrino, S.: Review of form-finding methods for tensegrity structures. Int. J. Space Struct. **18**(4), 209–223 (2003)
20 Kahla, N.B., Kebiche, K.: Nonlinear elastoplastic analysis of tensegrity systems. Eng. Struct. **22**(11), 1552–1566 (2000)

21 Murakami, H.: Static and dynamic analyses of tensegrity structures. Part II. Quasi-static analysis. Int. J. Solids Struct. **38**(20), 3615–3629 (2001)
22 Crane III, C.D., Duffy, J., Correa, J.: Static analysis of tensegrity structures. J. Mech. Design **127**(2), 257–268 (2005)
23 Bathe, K.J., Ramm, E., Wilson, E.: Finite element formulations for large deformation dynamic analysis. Int. J. Numer. Meth. Eng. **9**(2), 353–386 (1975)
24 Bathe, K.J., Ozdemir, H.: Elastic-plastic large deformation static and dynamic analysis. Comput. Struct. **6**(2), 81–92 (1976)
25 Bathe, K.J.: Finite Element Procedures. Englewood Cliffs, New Jersey: Prentice-Hall (1996)
26 Murakami, H.: Static and dynamic analyses of tensegrity structures. Part 1. Nonlinear equations of motion. Int. J. Solids Struct. **38**(20), 3599–3613 (2001)
27 Masic, M., Skelton, R., Gill, P.: Algebraic tensegrity form-finding. Int. J. Solids Struct. **42**(16-17), 4833–4858 (2005)
28 Deng, H., Kwan, A.S.K.: Unified classification of stability of pin-jointed bar assemblies. Int. J. Solids Struct. **42**(15), 4393–4413 (2005)
29 Zhang, J.Y., Ohsaki, M.: Adaptive force density method for form-finding problem of tensegrity structures. Int. J. Solids Struct. **43**(18-19), 5658–5673 (2006)
30 Ohsaki, M., Zhang, J.Y.: Stability conditions of prestressed pin-jointed structures. Int. J. Nonlinear Mech. **41**(10), 1109–1117 (2006)
31 Pellegrino, S., Calladine, C.R.: Matrix analysis of statically and kinematically indeterminate frameworks. Int. J. Solids Struct. **22**(4), 409–428 (1986)
32 Tran, H.C., Lee, J.: Advanced form-finding for cable-strut structures. Int. J. Solids Struct. **47**(14-15), 1785–1794 (2010)